Folding pathways to crumpling in thermalized elastic frames

D. Yllanes,[1,2,3,4,*] D.R. Nelson,[5] and M. J. Bowick[3]

[1] *Department of Physics and Soft Matter Program, Syracuse University, Syracuse, NY, 13244*
[2] *Chan Zuckerberg Biohub, San Francisco, CA 94158*
[3] *Kavli Institute for Theoretical Physics, University of California, Santa Barbara, CA 93106, USA*
[4] *Instituto de Biocomputación y Física de Sistemas Complejos (BIFI), 50009 Zaragoza, Spain*
[5] *Department of Physics, Department of Molecular and Cellular Biology and School of Engineering and Applied Sciences, Harvard University, Cambridge, MA 02138, USA*

(Dated: October 3, 2019)

The mechanical properties of thermally excited two-dimensional crystalline membranes can depend dramatically on their geometry and topology. A particularly relevant example is the effect on the crumpling transition of holes in the membrane. Here we use molecular dynamics simulations to study the case of elastic frames (sheets with a single large hole in the center) and find that the system approaches the crumpled phase through a sequence of origami-like folds at decreasing length scales when temperature is increased. We use normal-normal correlation functions to quantify the temperature-dependent number of folds.

I. INTRODUCTION

Studies of two-dimensional materials such as graphene [1] have stimulated renewed exploration of the statistical mechanics of elastic membranes. Thermalized elastic membranes [2, 3] have a low-temperature extended ("flat") phase with long-range order in the surface normals and a scale-dependent bending rigidity (κ) and Young's modulus (Y) [4–9]. Without strong distant self-avoidance these materials are also believed to undergo a crumpling transition when the microscopic bending rigidity is comparable to the scale of thermal fluctuations [3, 9–12]. The crumpling transition, however, has never been convincingly observed in a physical system. The challenge is to find a thin material that exhibits both the flat phase and the crumpled phase. One might expect that soft flexible systems, such as pure amphiphilic bilayers [13], would then be the natural setting to observe the transition from a flat phase to a crumpled phase. But here length scales become important. The flat phase itself is stabilized by the strong thermal stiffening of the bending rigidity resulting from soft flexural phonons that give rise to isotropic thermal corrugations. These fluctuations set in only above the thermal length scale, $\ell_{\rm th}$, beyond which the renormalization of the bending rigidity becomes comparable to the microscopic (bare) bending rigidity κ_0. This scale, which follows from the renormalization group flow of the bending rigidity, is given by $\ell_{\rm th} \sim \kappa_0/\sqrt{Y_0 k_B T}$, where Y_0 is the bare Young's modulus. Even for the diblock copolymers of Ref. [13], however, this length is relatively large, $\ell_{\rm th} \sim 300$ nm at room temperature. It is therefore difficult to fabricate soft systems large enough to harness these thermal effects. Graphene, on the other hand, has a thermal length scale of the order of nanometers at room temperature, making it possible to observe a crinkled flat phase [14, 15]. The difficulty now is accessing the crumpling transition which, considering that for graphene $\kappa_0 \approx 1.25$ eV [16], would occur at temperatures of order 50 000 K!

In [17] it was shown that the crumpling transition can be dramatically lowered by either perforating the membranes with a periodic array of holes or by excising a single large hole to form a thin frame. In both cases there are two effects which lower the crumpling temperature. There is less material to bend and there are fewer multiples of the thermal length scale contributing to the stiffening of the renormalized bending rigidity. For perforated membranes the growth is cut off by the mean

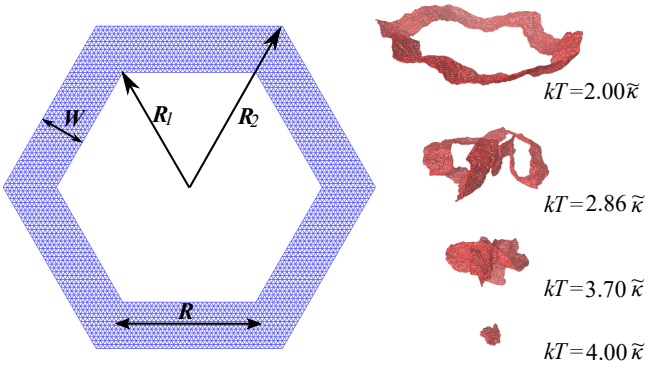

FIG. 1. Geometry of our system. We consider a hexagonal frame of inner radius R_1 and outer radius $R_2 = R_1 + W$, whose surface is triangulated. Each bond in the resulting lattice contains a spring potential, which characterizes the membrane's stretching, and each pair of neighboring triangles has a cosine interaction potential depending on the angle between their normals, characterized by a bending rigidity $\tilde{\kappa}$. See (1). As temperature is increased, the system transitions from an extended phase, with long-range order in the normals, to a crumpled phase. We show snapshots of the thermalized system at four temperatures.All images in this figure have $R_1 = 30$ and $R_2 = 42$.

* david.yllanes@czbiohub.org

spacing between holes and for thin frames by the narrow frame width. Here we explore crumpling for a thin hexagonal frame so as to preserve as many of the symmetries of the triangular lattice as possible. We find that crumpling is indeed enhanced, but also uncover a striking pathway to the crumpled phase. A well-known elementary bending mode is an origami-like fold along a line [18–20]. The energy cost for such a fold is proportional to the length of the fold line rather than the typical area cost for introducing a complex network of crinkles designed to crush a macroscopic piece of membrane [21, 22].

With our molecular dynamics simulations we find that crumpling occurs via a sequence of these soft origami folds. The successive stages of crumpling may be characterized by the distribution of the fold lines. The patterns observed correspond to the fold lines for the exactly solvable model of planar folding first studied in [19].

The rest of the paper is organized as follows: Section II presents our coarse-grained crystalline model and describes our simulations. In Section III we define an order parameter sensitive to the degree of crumpling based on normal-normal correlations and describe the folding process qualitatively. This description is made more quantitative in Section IV with the use of the full normal-normal correlation function. Finally, Section V examines the effect of changing the size of the hole and Section VI summarizes our conclusions. We include an appendix that considers the normal-normal correlation function in Fourier space.

II. MODEL

We consider a two-dimensional sheet of elastic material with a large hole in the center (a *frame*), which we model as a crystalline membrane [10]. In this representation, the sheet is discretized with a tiling of equilateral triangles of side $a = 1$, which defines a lattice of unbreakable but elastic bonds. In order both to facilitate triangulation and to approach a circular symmetry we use a hexagonal geometry with inner radius R_1 and outer radius $R_2 = R_1 + W$ (Figure 1). This system can be regarded as six ribbons of length $R = (R_1 + R_2)/2$ stitched together to form a hexagon. On this triangular lattice we define a standard coarse-grained elastic Hamiltonian [23]:

$$\mathcal{H} = \mathcal{H}_{\text{stretch}} + \mathcal{H}_{\text{bend}}, \tag{1}$$

where

$$\mathcal{H}_{\text{stretch}} = \frac{1}{2}\epsilon \sum_{\langle i,j \rangle} (r_{ij} - a)^2, \tag{2}$$

$$\mathcal{H}_{\text{bend}} = \tilde{\kappa} \sum_{\langle \alpha,\beta \rangle} (1 - \hat{\boldsymbol{n}}_\alpha \cdot \hat{\boldsymbol{n}}_\beta) \tag{3}$$

The sum in the stretching term is over all pairs of lattice nearest neighbors $\langle i, j \rangle$. The bending energy, on the other hand, depends on the angles between the normals $\boldsymbol{n}_\alpha$, $\boldsymbol{n}_\beta$ of all pairs of triangles (α, β) that share a side. Each of these pairs of triangles defines a dihedral, which is how we will refer to each term in the bending Hamiltonian in the rest of the paper.

The coupling constants ϵ and $\tilde{\kappa}$ are directly related to the Young's modulus and bare bending rigidity of continuum elastic theory ($Y_0 = 2\epsilon/\sqrt{3}$, $\kappa_0 = \sqrt{3}\tilde{\kappa}/2$ [23]). As temperature increases, the frame transitions from a thermally excited flat phase, with long-range order in the normals, to a crumpled phase (see Figure 1). This crumpling transition has already been thoroughly studied for unperforated sheets [3, 7, 9–12] as well as for sheets with perforations [17]. In the following, therefore, we do not focus on the crumpling transition itself, but instead study an intermediate regime, where we show that crumpling is realized through a series of folding pathways.

Aside from an overall constant factor that defines the energy units, what differentiates one elastic material from another is the ratio $\epsilon/\tilde{\kappa}$. Following [17, 24] we set $\epsilon = 1440\tilde{\kappa}/a^2$, which approximates graphene values without making the system too rigid and hard to thermalize. In practice, this choice makes very little difference in the final results, since the crumpling point depends only logarithmically on the Young's modulus (see, e.g., [25] and compare the crumpling temperatures in [12] and [17]).

We have carried out Molecular Dynamics simulations of model (1) for different system sizes and a wide temperature range (working in an NVT ensemble with a standard Nosé-Hoover thermostat [26, 27]). Our simulations were implemented in the HOOMD-blue package [28, 29] and run on Tesla GPUs. Following [17], we use a timestep of $\Delta t = 0.0025\tau$, where $\tau = \sqrt{ma^2/kT}$ is the Lennard-Jones unit of time (expressed in terms of the particle mass m) and we use natural units with $a = m = 1$. All energies are measured in units of kT. For each system size and temperature we run for 10^9 MD steps and use a jackknife procedure [30] to estimate statistical errors. For our larger frames with $R_1 = 70, R_2 = 82$ these runs take from 60 to 70 hours on a Tesla K40m GPU.

III. THE CRUMPLING ORDER PARAMETER

The standard method to study the crumpling transition itself is to consider the radius of gyration of the frame

$$\mathcal{R}_{\text{g}}^2 = \frac{1}{3N} \sum_{i=1}^{N} \langle \boldsymbol{R}_i \cdot \boldsymbol{R}_i \rangle, \quad \boldsymbol{R}_i = \boldsymbol{r}_i - \boldsymbol{r}_{\text{center of mass}}. \tag{4}$$

In this equation and in the following, $\langle \cdot \rangle$ will denote a thermal average. At low temperatures, $\mathcal{R}_{\text{g}}^2 \sim R_2^2$, while in the crumpled phase $\mathcal{R}_{\text{g}}^2 \sim \log(R_2/a)$. Panels (a) and (b) of Figure 2 show $\mathcal{R}_{\text{g}}$ as a function of temperature for two frame sizes.

A very clear signal of the phase transition can also be obtained by plotting the specific heat C of our elastic

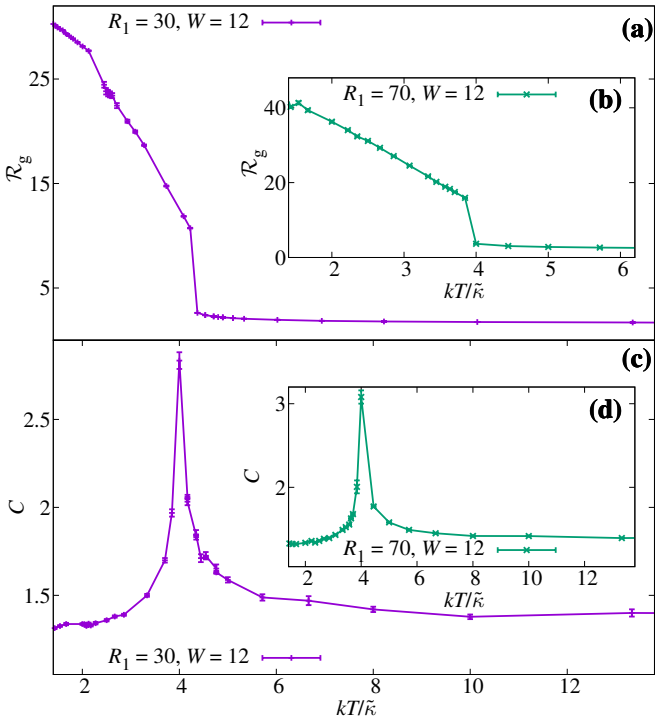

FIG. 2. The crumpling transition of a frame. We plot the radius of gyration, Eq. (4), as a function of temperature for a frame of $R_1 = 30$ and $R_2 = 42$ ($W = 12$) in panel (a). Panel (b) shows the corresponding curve for a hexagon of $R_1 = 70$ and the same width $W = 12$. For the same systems, we plot the specific heat C in panels (c) and (d). This quantity has a sharp peak at the transition point, $kT_c/\tilde{\kappa} \approx 4.00$ for both sizes.

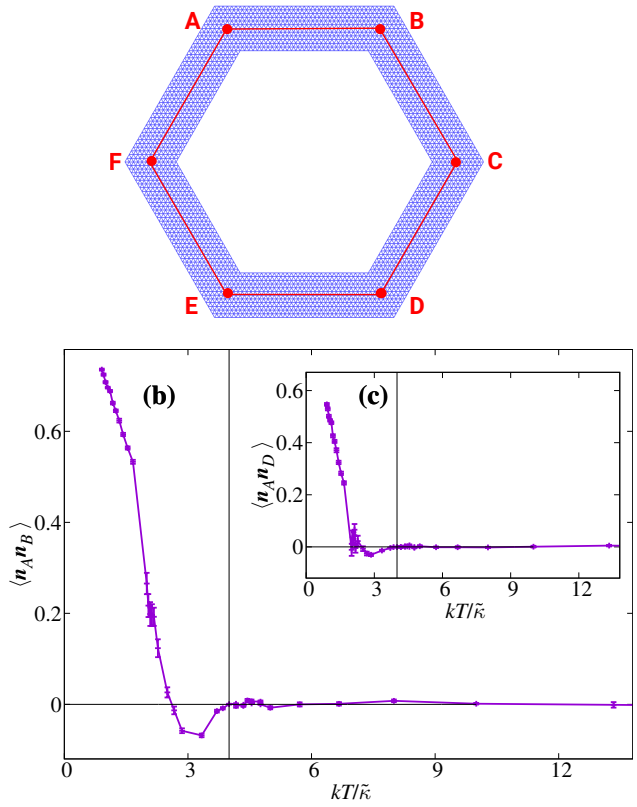

FIG. 3. We will consider the correlation between the red points along the central hexagon of radius $R = (R_1 + R_2)/2$ (a). In panel (b) we plot of the correlation $\langle \boldsymbol{n}_A \cdot \boldsymbol{n}_B \rangle$ between normals at opposing vertices along the same side of the hexagon (we consider the average of the six equivalent pairs of points). This correlation goes to zero well before the critical point $kT_c \approx 4.00\tilde{\kappa}$ identified in Figure 2 (marked with a vertical line) and in fact becomes negative, indicating an anticorrelation between normals. Inset (c) shows the corresponding graph for diagonally opposed vertices, $\langle \boldsymbol{n}_A \cdot \boldsymbol{n}_D \rangle$ (and two equivalent pairs), which goes to zero even earlier but is much noisier.

frames a function of temperature, which can be computed with a fluctuation-response formula [17]:

$$C = \frac{1}{N}\left(\langle \mathcal{H}^2 \rangle - \langle \mathcal{H} \rangle^2\right) . \tag{5}$$

This quantity has a very sharp peak at the transition point of $kT_c \approx 4.0\tilde{\kappa}$ for both values of R_1 studied (see Figures 2c and d).

Finite-size scaling studies of the crumpling transition have already been done in considerable detail both for pristine [12] and perforated [17] sheets. Here, we are interested in following the detailed geometry of the frame as the transition is approached. To this end, we have found that a system size of $R_1 = 30$ and $R_2 = 42$ provides a good compromise: The frame is large enough for finite-size effects to be negligible (compare the position of the peaks for $R_1 = 30$ and $R_1 = 70$ in Figure 2) and to provide good statistics, yet small enough for us to follow individual folds and creases in snapshots. In what follows we shall always consider this particular system size.

Even though $\mathcal{R}_g$ is a useful proxy for a crumpling order parameter, it is illuminating to study normal-normal correlations directly. Because our frames are made up of six ribbons of length $R = (R_1 + R_2)/2$ stitched together to form a hexagon (see Fig. 1) we first consider a long elastic ribbon at a low temperature. Then the correlation between the normal at the beginning (O) and end (X) of the ribbon is [25]

$$\langle \hat{\boldsymbol{n}}_O \cdot \hat{\boldsymbol{n}}_X \rangle_L = 1 - \frac{kT}{2\pi\kappa_0}\left[\eta^{-1} + \log\left(\frac{\ell_{\rm th}}{a}\right) + \mathcal{C}\frac{kT}{\kappa_0}\left(\frac{\ell_{\rm th}}{L}\right)^{\eta}\right] . \tag{6}$$

In this equation, $\eta \approx 0.8$ is a critical exponent, $\mathcal{C}$ is a positive constant of order unity and $\ell_{\rm th}^2 = 2\sqrt{3}\pi^3\tilde{\kappa}^2/3kT\epsilon$ is the thermal length scale. For sufficiently small kT, this correlation is positive even for $r_{OX} = L \to \infty$. Conversely, we could in principle approximate the crumpling transition as the point where $\langle \boldsymbol{n}_O \cdot \boldsymbol{n}_X \rangle \approx 0$ for large $r_{OX} = L$.

This test is easily done by considering our frame to be a ribbon of width $R_2 - R_1 = W$, with periodic boundary conditions in the azimuthal direction. If we then consider a central hexagon of radius $R = (R_1 + R_2)/2$, we can identify $\langle \boldsymbol{n}_O \cdot \boldsymbol{n}_X \rangle$ with $\langle \boldsymbol{n}_A \cdot \boldsymbol{n}_D \rangle$, the correlation between

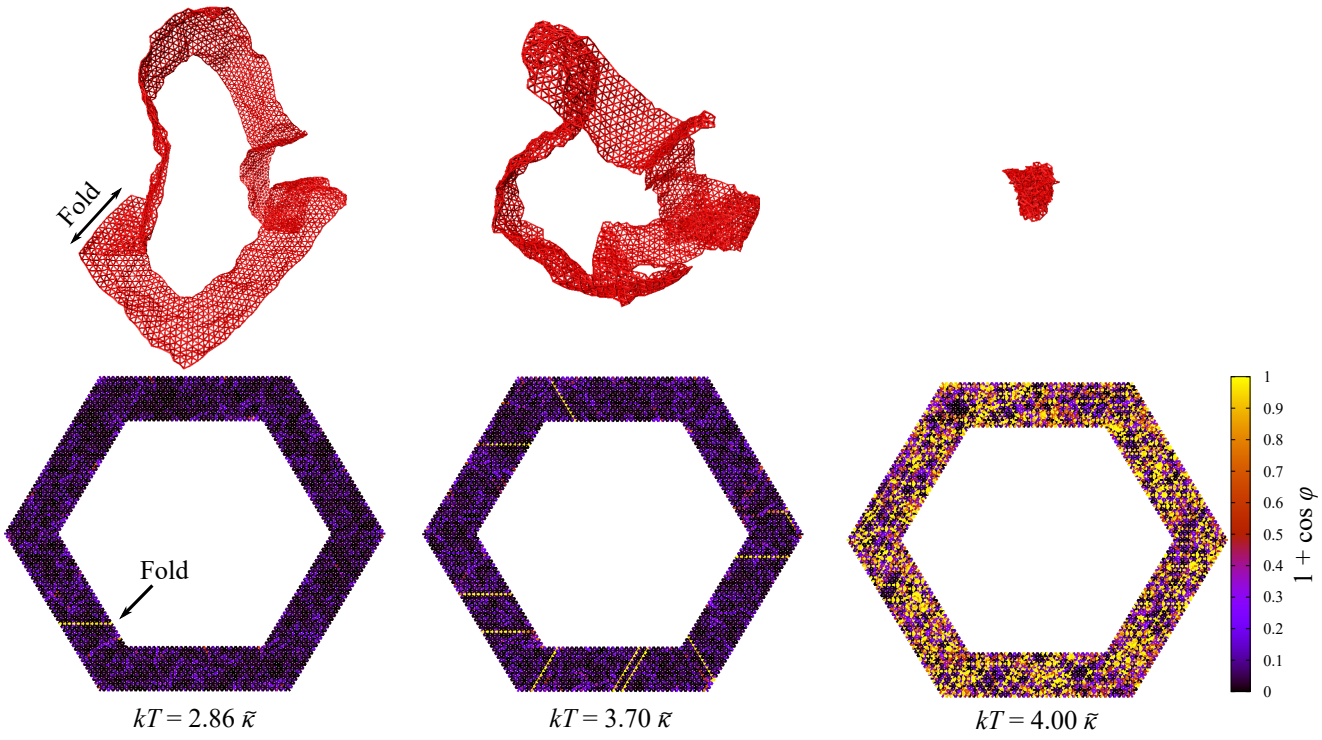

FIG. 4. Heat map of bending energy on a hexagonal frame with various degrees of crumpling. For three temperatures we show two representations of a typical thermalized configuration. On the top row we simply show the three-dimensional state of the sheet. On the bottom row, we plot via a heat map the value of $(1 + \cos\varphi)$ for all the dihedrals in the system, where φ is the angle between normals ($\varphi = \pi$ for a flat dihedral, where the energy is minimal). This quantity is a measure of the bending energy (3) in natural units. For the lowest temperature shown, $kT = 2.86\tilde{\kappa}$, most of the energy is concentrated in a single sharp fold. As we approach the critical point of $kT_c \approx 4.0\kappa$, an increasing number of well-defined radial folds appear.

diagonally opposed vertices (see Figure 3) [31].

If we plot $\langle \boldsymbol{n}_A \cdot \boldsymbol{n}_D \rangle$ as a function of temperature, however, we find that it goes to zero well before the crumpling temperature of $kT_c \approx 4.0\tilde{\kappa}$, although the data is rather noisy. We can obtain a better plot by studying instead the correlation between opposing vertices along the same side of the hexagon ($\langle \boldsymbol{n}_A \cdot \boldsymbol{n}_B \rangle$ and five symmetric equivalents). This quantity goes to zero at a higher temperature than $\langle \boldsymbol{n}_A \cdot \boldsymbol{n}_D \rangle$, but still well before the actual crumpling transition. Furthermore, for a finite temperature range, $\langle \boldsymbol{n}_A \cdot \boldsymbol{n}_B \rangle$ is negative, indicating anticorrelation between normals.

Let us consider the meaning of this negative correlation. The easiest way to achieve $\boldsymbol{n}_A \cdot \boldsymbol{n}_B = -1$ is to create a single fold between the two points. Of course, our frame is fluctuating thermally. A measurable negative ensemble averaged $\langle \boldsymbol{n}_A \cdot \boldsymbol{n}_B \rangle$, however, suggests that typical instantaneous configurations of the frame might have well defined origami folds, separated by a distance comparable to $|\boldsymbol{r}_A - \boldsymbol{r}_B|$, but whose location varies with time. Upon recalling that the correlation for the even more distant points such as A and D goes to zero at an even lower temperature [Figure 3-(c)], we can hypothesize that there exists an intermediate regime before crumpling where the system concentrates its bending energy on a small number of well-defined folds. We expect that the distance between single folds is a function of temperature, which becomes quite small as T approaches the crumpling transition.

We can test this idea of a temperature-dependent folding scale by plotting a heat map of bending energy on the frame (Figure 4). For low temperatures, there is hardly any bending energy in the system. As T is increased, we find that almost all the bending energy is concentrated in one or two radial segments, indicating well-defined creases. The number of such folds increases with temperature until, at the crumpling transition $kT_c \approx 4.0\tilde{\kappa}$, the whole system is crumpled (i.e., folded at a microscopic scale).

IV. NORMAL-NORMAL CORRELATION FUNCTION

We can make the analysis more quantitative by studying $\hat{\boldsymbol{n}}(r)$, the normal to the sheet along the central hexagon of radius $R = (R_1 + R_2)/2$, as a function of

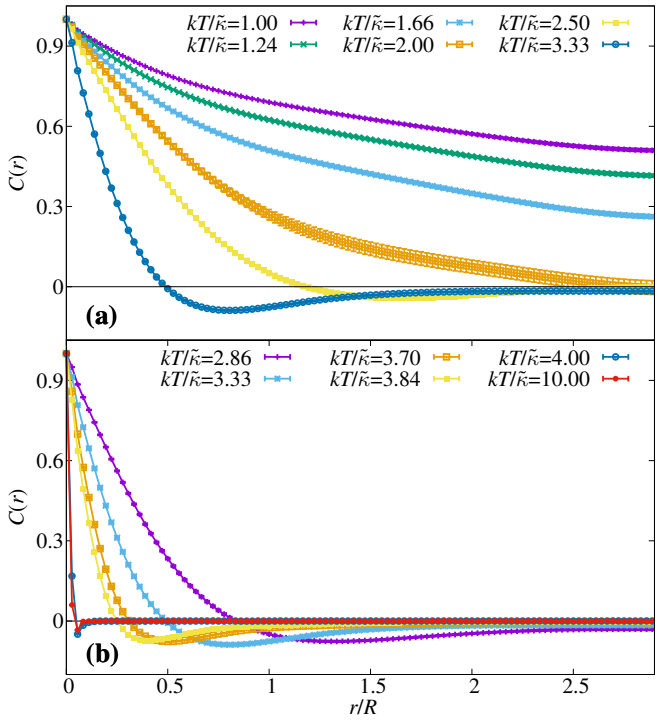

FIG. 5. Normal-normal correlation as a function of the arc length r along the central hexagon of Figure 3 for many temperatures from the flat into the crumpled phase ($R_1 = 30, W = 12$ and hence $R = 36$). For low temperatures, the correlation function exhibits long-range order and does not go to zero at long distances. As we approach the critical point of $kT_c \approx 4.00\ \tilde{\kappa}$, the correlation function goes to zero for finite r and reaches a well-defined negative minimum, indicating the typical length scale of the folds in the system. At $kT \geq 4.00\tilde{\kappa}$, the folds occur at a microscopic scale, so the only anticorrelation happens for the distance given by our discretization (i.e., between vertices at opposing ends of the same dihedral).

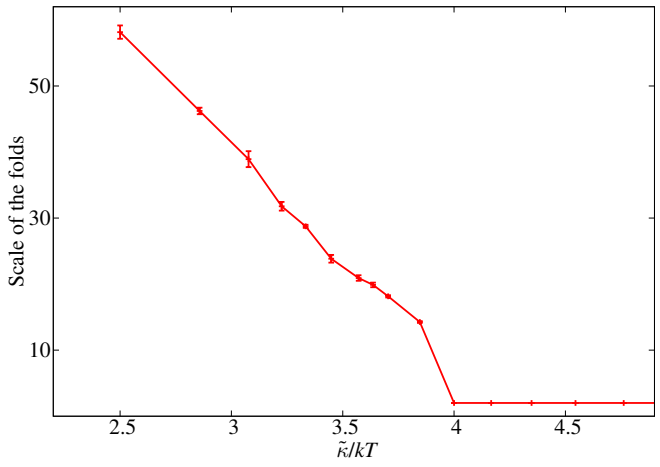

FIG. 6. Scale of the folds as a function of temperature. We plot the position of the minimum of $C(r)$ in (Figure 5) for each temperature, showing how the distance between folds decreases as we approach the crumpling point. For $kT \lesssim 2.4\tilde{\kappa}$ the minimum disappears and $C(r)$ becomes monotonic.

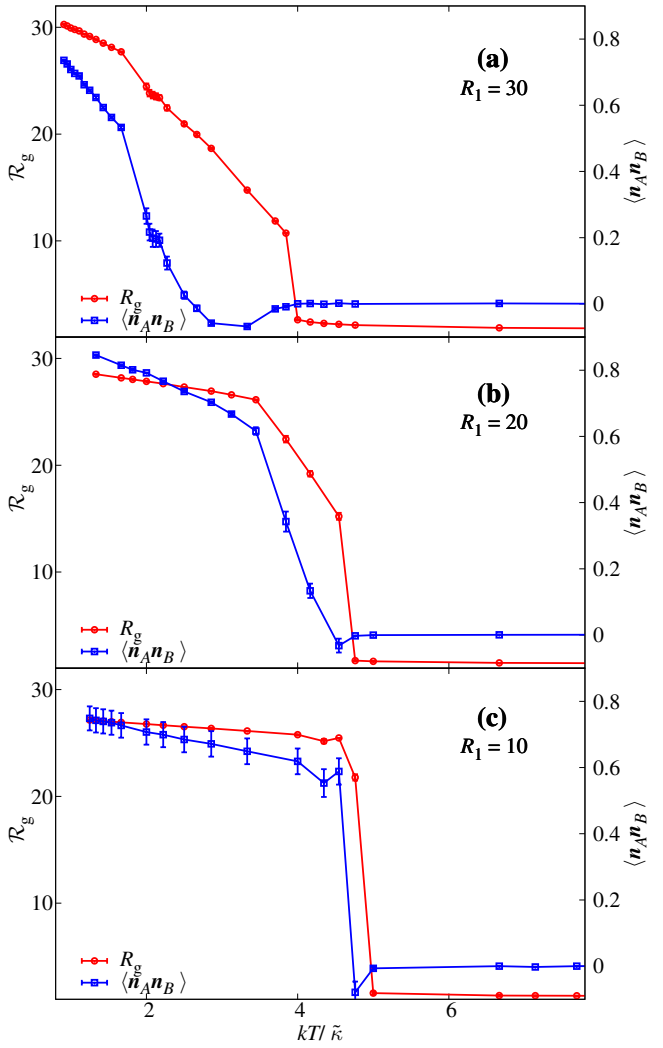

FIG. 7. Effect of the frame width on the folding regime. We show the radius of gyration $\mathcal{R}_g$ (left axis, circles) and the normal-normal correlations $\langle \boldsymbol{n}_A \cdot \boldsymbol{n}_B \rangle$ (right axis, squares) for three different geometries. The outer radius is fixed at $R_2 = R_1 + W = 42$, with $R_1 = 30$ (a), $R_1 = 20$ (b) and $R_1 = 10$ (c). The temperature interval between the point where $\langle \boldsymbol{n}_A \cdot \boldsymbol{n}_B \rangle = 0$ and the crumpling transition is a visual representation of the shrinking folding regime as W increases.

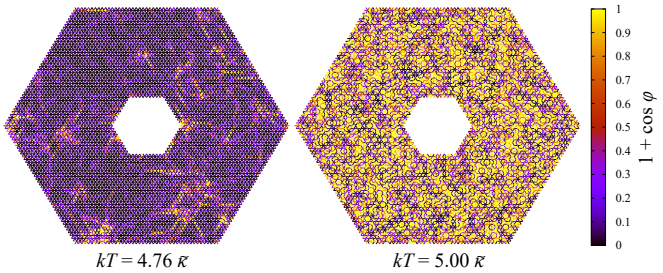

FIG. 8. As in Figure 4, but now for a much thicker frame ($W = 32$). The system suddenly transitions from being almost flat with some localized larger fluctuations to being completely crumpled. We cannot identify the same individual folds as for the thin frame.

the arc length. Then we can compute

$$C(r) = \sum_s \langle \hat{\boldsymbol{n}}(s) \cdot \hat{\boldsymbol{n}}(s+r) \rangle. \quad (7)$$

This function gives us more complete information than the correlation between particular pairs of points of the previous section and is also more precise, since we can average over the whole curve of annular midpoints around the hexagon.

The result for $R_1 = 30$, $R_2 = 42$ is plotted in Figure 5, where several regimes can be identified. At the lowest temperatures, the system is deep in the flat phase and $C(r)$ has a positive asymptote as $r \to \infty$. At the highest temperatures, in the crumpled phase, $C(r)$ is trivial: it is negative for $r = 2$ (opposite vertices of one dihedral) and zero beyond that since the system is folded at a microscopic scale. Qualitatively similar behavior was observed, e.g. [11], for tethered surfaces with the geometry of a parallelogram. Our interest here is the existence of an intermediate regime where $C(r)$ has negative values for a finite r window, which shifts and shrinks as T approaches T_c. Just prior to this anomalous behavior, we find that $C(r)$ is well described by an exponential decay $C(r) \simeq \exp(-r/\ell_p)$, where ℓ_p is a persistence length (see, e.g. [17, 25, 27]). See the curves with $kT/\tilde{\kappa} \leq 2.00$ in Figure 5.

Since the $C(r)$ are very smooth functions and can be measured to high precision, we can easily find a minimum for each one in the folding regime. This minimum then indicates the average distance between folds (or, alternatively, their average number) for each temperature (Figure 6).

V. ROLE OF THE SYSTEM GEOMETRY

As we have mentioned, the $C(r)$ function has been extensively studied for unperforated membranes. In these cases, there is no folding regime and the system suddenly switches between a flat phase where $C(r) > 0$ for all r and an extremely compact crumpled phase where $C(r = 2) < 0$ and $C(r > 2) = 0$. This behavior arises because in unperforated membranes the system presumably cannot find a privileged direction along which to fold in order to minimize its bending energy.

We have tested these ideas by redoing our simulations for thicker frames (smaller holes). In particular, keeping $R_2 = 42$, we have run simulations for $R_1 = 10, 20$ ($W = 22, 32$, respectively, compared with the $W = 12$ studied above). In this analysis, we have found that for $W = 22$ a folding regime can still be identified (though it spans a much narrower temperature interval than for $W = 12$), while for $W = 32$ the behavior is already qualitatively the same as for sheets without a hole [32].

This study is summarized in Figures 7 to 9. First, Figure 7 plots the radius of gyration and $\langle \boldsymbol{n}_A \cdot \boldsymbol{n}_B \rangle$ for the three frame widths. As discussed in the previous sections, the interval between the temperature at which

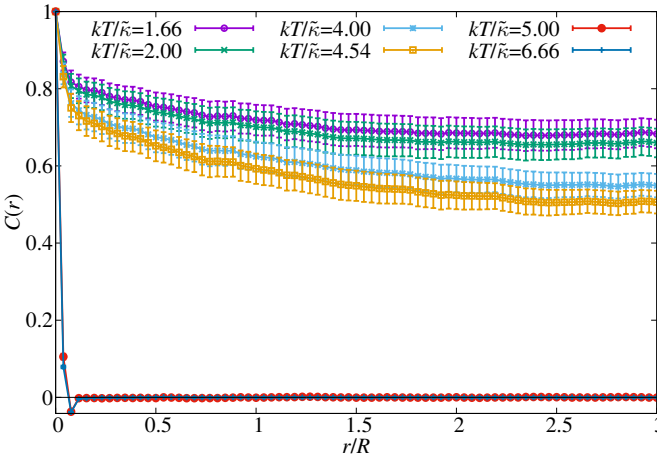

FIG. 9. Normal-normal correlation function as in Figure 5, but for a very thick frame ($R_1 = 10$, $R_2 = 42$). Now we cannot identify an intermediate regime between the flat and crumpled phases showing anticorrelation (folds) at finite distances.

$\langle \boldsymbol{n}_A \cdot \boldsymbol{n}_B \rangle = 0$ (appearance of very large folds) and T_c corresponds to the folding regime. This is very wide for $W = 12$, noticeably narrower for $W = 22$ and has essentially disappeared for $W = 32$.

Moreover, if we consider (Figure 8) the same bending energy heat map we used for our original frames, we see that even at a temperature just 5% below T_c no folds can be identified for our $W = 32$ frame. The would-be folding regime has already shrunk beyond our ability to detect it. Finally, the picture is confirmed by considering $C(r)$ again in Figure 9, where the correlation functions suddenly change from having a positive asymptotic value (flat phase) to collapsing completely. This is the same pattern observed for membranes without holes in Ref. [11].

VI. CONCLUSIONS

We have studied the equilibrium configurations of thermalized elastic frames as temperature is increased and found that, as the crumpling transition is approached, most of the bending energy is concentrated on a growing number of origami-like folds. The scale of these folds is a well-defined function of temperature.

The folding pathway explored here neglects distant self-avoidance. In Ref. [17] we argued that the crumpling transition studied here for phantom frames with large holes would persist even in the presence of self-avoidance in an appropriate thermodynamic limit. The non-trivial width-dependent scaling of the thermally generated renormalized persistence length associated with our hexagonal frames

$$\ell_p = \frac{2W\kappa^R(W)}{kT}, \quad \kappa^R(W) = \kappa_0 \left(\frac{W}{\ell_{th}}\right)^{\eta}, \quad \eta \approx 0.8, \quad (8)$$

suggests that the appropriate limit is $R, W \to \infty$ with fixed $W(W/\ell_{\rm th})^{\eta}/R$ for frames with width W and edge length R. Thus, we expect that a sharp transition survives for hexagonal frames, where both a crumpled and a flat phase would survive in a polymer-like large-size limit. In addition, we expect that the origami-like folding pathway uncovered here will not be significantly affected by distant self-avoidance for most of the run-up to the crumpling transition from low temperatures. Indeed, few self-intersections are evident in the partially crumpled images shown in Figs. 1 and 4. How self-avoidance affects the folding at the transition itself when $kT \approx 4.0\tilde{\kappa}$ is an interesting subject for future investigation.

Some insight into the effect of self-avoidance on folding patterns without holes follows from the study of Vliegenthart and Gompper of forced crumpling of self-avoiding elastic sheets at zero temperature [21]. Here, a comparison of gradual forced crumpling with and without self-avoidance eventually reveals a radial bias, just as we find here with a single large hole. The patterns of wrinkles in this computer experiment are qualitatively similar for both phantom and self-avoiding membranes.

ACKNOWLEDGMENTS

This research was supported by the NSF through the DMREF grant DMR-1435794 and DGE-1068780, as well as by the Syracuse University Soft Matter Program. Work by DRN was also supported through the NSF DMREF program, via NSF grant DMR-1435999 and via the Harvard Materials Science Research and Engineering Center, through NSF grant DMR-1420570. The research of MJB was supported in part by the National Science Foundation under Grant No. NSF PHY-1748958. DY thanks the KITP for hospitality during part of this project and acknowledges funding by Ministerio de Economía, Industria y Competitividad (MINECO) (Spain) through grants no. FIS2015-65078-C2 and PGC2018-094684-B-C21 (also partly funded by the EU through the FEDER program) and the resources and assistance provided by BIFI-ZCAM (Universidad de Zaragoza), where we carried out most of our simulations on the Cierzo supercomputer.

Appendix A: The normal-normal correlation in Fourier space

In the main part of this paper we have worked with the correlation function in real (position) space. However, its Fourier transform

$$F(k) = \left\langle \left| \sum_r C(r) \mathrm{e}^{\mathrm{i}kr} \right|^2 \right\rangle \qquad \text{(A1)}$$

provides an interesting complementary picture. Now the folding regime leads to a *maximum* in $F(k)$ that shifts to smaller wavenumbers as T increases (Figure 10). In addition, considering $F(k)$ as a function of temperature offers an alternative way of finding the crumpling point (Figure 11).

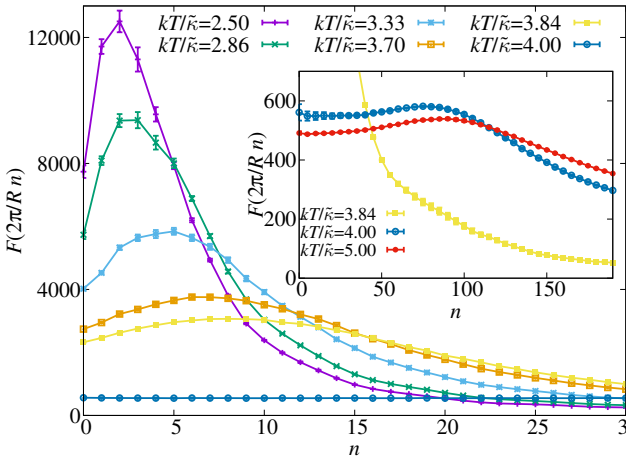

FIG. 10. We plot the full normal-normal correlation function in Fourier space, defined by Eq. (A1), for several temperatures. Since in our discretized system, the only available spatial wavevectors are $k_n = n(2\pi/R)$, in this case we show the results for a larger system than in previous figures ($R_1 = 70, W = 12, R = 76$). There is a well-defined maximum for each temperature in the extended phase and a dramatic transition in the shape of the function once we reach the crumpling temperature $kT_{\rm c} \approx 4.0\kappa$. The *inset* shows a closeup of the structure function as we move deep into the crumpled phase (note the scales of the axes).

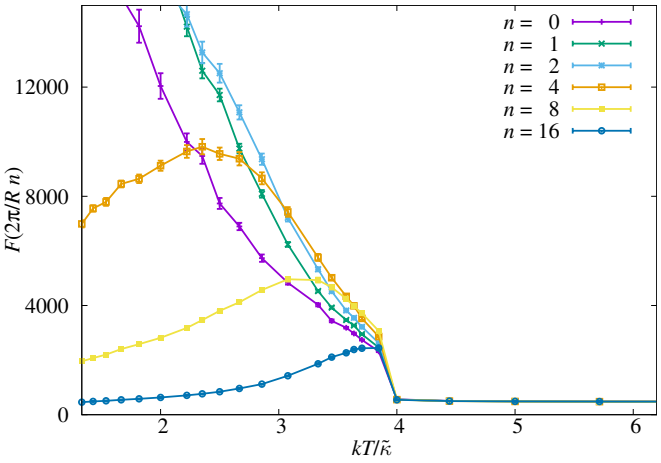

FIG. 11. The zeroth component of the correlation function (A1), $F(k = 0)$, is also a good order parameter for the crumpling transition. Here, we plot this and other components of F as a function of temperature.

Appendix B: The crumpling process

In the main text of the paper, we considered the folding pathways as the temperature was increased up to

the crumpling transition, which we studied through the analysis of configurations extracted from the equilibrium evolution of the system. We can obtain a complementary picture by studying the non-equilibrium evolution of a system at T_c which started from a completely flat configuration. We have done this in Figures 12 and 13 for our systems with $R_2 = 42$ and $R_1 = 10, 30$ (each at their corresponding T_c). For the latter, individual folds quickly appear at several points along the frame and serve to nucleate crumpled regions. It takes longer for the thicker frame to crumple, since the system cannot create linear folds that easily. In both cases, once the system has crumpled completely, the microscopic fold patterns correspond to those of the planar folding problem, as in [19].

[1] M. I. Katsnelson, *Graphene: Carbon in Two Dimensions* (Cambridge University Press, New York, 2012).
[2] D. R. Nelson, *Defects and Geometry in Condensed Matter Physics* (Cambridge University Press, Cambridge,UK, 2002).
[3] D. Nelson, T. Piran, and S. Weinberg, *Statistical Mechanics of Membranes and Surfaces*, 2nd ed. (World Scientific, Singapore, 2004).
[4] D. Nelson and L. Peliti, J. Phys. France **48**, 1085 (1987).
[5] J. A. Aronovitz and T. C. Lubensky, Phys. Rev. Lett. **60**, 2634 (1988).
[6] E. Guitter, F. David, S. Leibler, and L. Peliti, Journal de Physique **50(14)**, 1787 (1989).
[7] P. Le Doussal and L. Radzihovsky, Phys. Rev. Lett. **69**, 1209 (1992).
[8] Z. Zhang, H. T. Davis, and D. M. Kroll, Phys. Rev. E **48**, R651 (1993).
[9] M. J. Bowick, S. M. Catterall, M. Falcioni, G. Thorleifsson, and K. N. Anagnostopoulos, J. Phys. I France **6**, 1321 (1996).
[10] M. J. Bowick and A. Travesset, Phys. Rep. **344**, 255 (2001).
[11] Y. Kantor and D. R. Nelson, Phys. Rev. A **36**, 4020 (1987).
[12] R. Cuerno, R. Gallardo Caballero, A. Gordillo-Guerrero, P. Monroy, and J. J. Ruiz-Lorenzo, Phys. Rev. E **93**, 022111 (2016).
[13] H. C. Shum, J. W. Kim, and D. A. Weitz, J.Am.Chem.Soc. **130**, 9543 (2008).
[14] R. Nicholl, H. J. Conley, N. V. Lavrik, I. Vlassiouk, Y. Puzyrev, V. P. Sreenivas, S. T. Pantelides, and K. I. Bolotin, Nat. Comm. **6**, 8989 (2015).
[15] M. K. Blees, A. W. Barnard, P. A. Rose, S. P. Roberts, K. L. McGill, P. Y. Huang, A. R. Ruyack, J. W. Kevek, B. Kobrin, D. A. Muller, and P. L. McEuen, Nature **524**, 204 (2015).
[16] A. Fasolino, J. H. Los, and M. I. Katsnelson, Nat. Mat. **6**, 858 (2007).
[17] D. Yllanes, S. S. Bhabesh, D. R. Nelson, and M. J. Bowick, Nat. Comm. **8**, 1381 (2017).
[18] Y. Kantor and M. V. Jaric, Europhys. Lett. **26**, 455 (1990).
[19] P. Di Francesco and E. Guitter, Europhys. Lett. **26**, 455 (1994).
[20] C. D. Santangelo, Annu. Rev. Condens. Matter Phys. **8**, 165 (2017).
[21] G. A. Vliegenthart and G. Gompper, Nat. Mat. **5**, 216 (2006).
[22] Y. Lahini, O. Gottesman, A. Amir, and S. M. Rubinstein, Phys. Rev. Lett. **118**, 085501 (2017).
[23] H. S. Seung and D. R. Nelson, Phys. Rev. A **38**, 1005 (1988).
[24] M. J. Bowick, A. Kosmrlj, D. R. Nelson, and R. Sknepnek, Phys. Rev. B **95**, 104109 (2017).
[25] A. Košmrlj and D. R. Nelson, Phys. Rev. B **93**, 125431 (2016).
[26] S. Nosé, The Journal of Chemical Physics **81**, 511 (1984).
[27] W. G. Hoover, Phys. Rev. A **31**, 1695 (1985).
[28] J. Glaser, T. D. Nguyen, J. A. Anderson, P. Lui, F. Spiga, J. A. Millan, D. C. Morse, and S. C. Glotzer, Comp. Phys. Comm. **192**, 97 (2015).
[29] J. A. Anderson, C. D. Lorenz, and A. Travesset, J. Comp. Phys. **227**, 5342 (2008).
[30] D. J. Amit and V. Martin-Mayor, *Field Theory, the Renormalization Group, and Critical Phenomena*, 3rd ed. (World Scientific, Singapore, 2005).
[31] We actually consider the average of $\langle \boldsymbol{n}_A \cdot \boldsymbol{n}_D \rangle$, $\langle \boldsymbol{n}_B \cdot \boldsymbol{n}_E \rangle$ and $\langle \boldsymbol{n}_C \cdot \boldsymbol{n}_F \rangle$.
[32] And quantitatively very similar, with kT_c approaching the value without a hole, although, unlike for our thin frames, in this case finite-size effects in kT_c are noticeable.

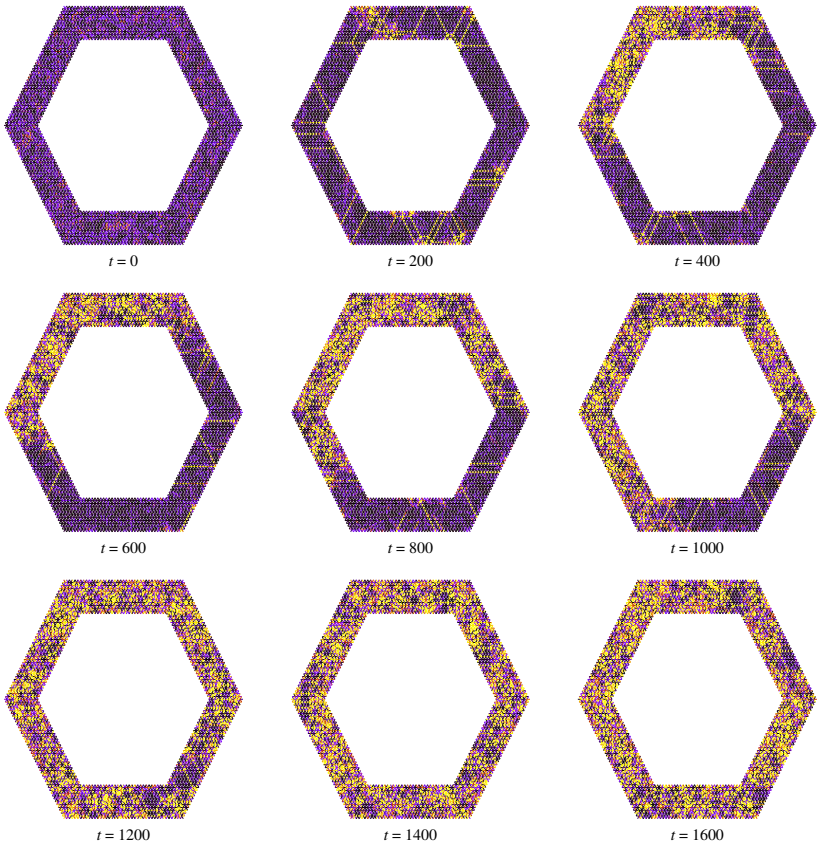

FIG. 12. Time evolution of the bending energy with $R_1 = 30$, $R_2 = 42$ at the crumpling transition $kT = 4.00\tilde{\kappa} \approx kT_c$ (times are in units of 10^4 MD steps). Note that linear folds appear in portions of the frame at intermediate times along this pathway.

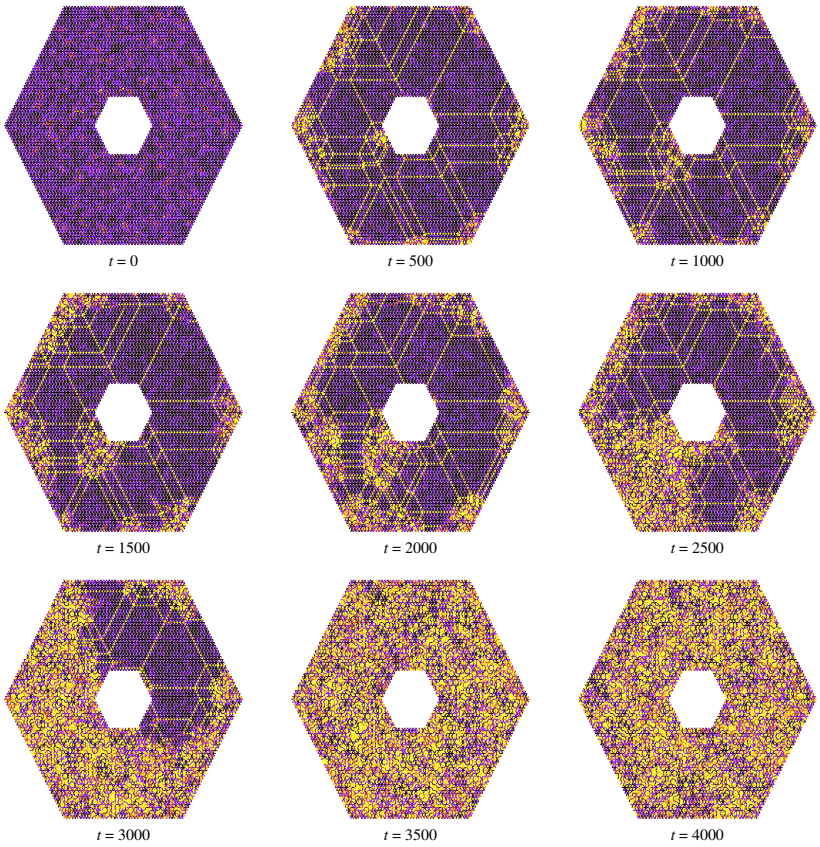

FIG. 13. Time evolution of the crumpling transition of a frame with a smaller hole, $R_1 = 10$, $R_2 = 42$. Here the crumpling transition occurs at a higher temperature and we set $kT = 5.00\tilde{\kappa} \approx T_c$.